CHAPTER

26

Modeling cellular shape changes in the presence of curved membrane proteins and active cytoskeletal forces

Mitja Drab[1], *Raj Kumar Sadhu*[2], *Yoav Ravid*[2], *Aleš Iglič*[1,3], *Veronika Kralj-Iglič*[4,5] *and Nir S. Gov*[2]

[1]Laboratory of Physics, Faculty of Electrical Engineering, University of Ljubljana, Ljubljana, Slovenia [2]Department of Chemical and Biological Physics, Weizmann Institute of Science, Rehovot, Israel [3]Laboratory of Clinical Biophysics, Faculty of Medicine, Department of Orthopedics, University of Ljubljana, Ljubljana, Slovenia [4]Laboratory of Clinical Biophysics, Faculty of Medicine, University of Ljubljana, Ljubljana, Slovenia [5]Laboratory of Clinical Biophysics, Faculty of Health Sciences, University of Ljubljana, Ljubljana, Slovenia

26.1 Introduction

The main element of biological membranes is the lipid bilayer with embedded inclusions such as proteins and different species of lipids (Cevc & Marsh, 1987; Israelachvili, 2011). Biological membranes can be viewed as a complex multicomponent system (Baumgart et al., 2011), composed of lipid molecules, proteins, carbohydrates, and many other biologically active components (Sackmann, 1990).

Membrane shape depends on the intrinsic shape of the membrane's molecular constituents and their interactions with other components, such as membrane skeleton and cytoskeleton. It has been shown that a nonhomogeneous lateral distribution and phase separation of membrane inclusions may be a driving force of cell shape transformations and necessary for the stabilization of highly curved membrane structures (Božič et al., 2006; Drab et al., 2019; Fošnarič et al., 2006, 2019; Gov, 2018; Hägerstrand et al., 2006; Iglič, Babnik, et al., 2007; Iglič, Lokar, et al., 2007; Kralj-Iglič et al., 1999; Leibler, 1986; Markin, 1981; Veksler & Gov, 2007).

Additionally, the shapes of cells may be also influenced by the forces exerted on the membrane by the cytoskeleton (Boulbitch, 1998; Discher, 2018; Evans & Skalak, 1980; Iglič, 1997;

DOI: https://doi.org/10.1016/B978-0-323-89911-6.00002-9

Iglič et al., 1998; Kozlov et al., 2014; Lim HW et al., 2002; Mohandas & Evans, 1994; Veksler & Gov, 2007). Among these are ATP-consuming active forces important for different cell functions. These include, for example, protrusive forces due to actin polymerization and contractile forces due to myosin molecular motor activity (Alimohamadi et al., 2020; Gov, 2018; Graziano et al., 2019; Penič, Fošnarič, et al., 2020; Rodríguez-García et al., 2015; Smith et al., 2018). Consequently, new theoretical approaches for modeling changes in the cell shape as a consequence of energy-consuming active forces have recently been developed (Fošnarič et al., 2019; Gov, 2018; Graziano et al., 2019; Penič, Fošnarič, et al., 2020; Rodríguez-García et al., 2015).

Cells also adhere to extracellular substrates which further affects their shape. The cellular adhesion over a substrate involves an initial stage of nonspecific and weak adhesion, followed usually by spreading that is driven by the formation of thin sheet-like lamellipodia (Cavalcanti-Adam et al., 2007; Cuvelier et al., 2007; Döbereiner et al., 2004; Gauthier et al., 2011). These lamellipodia formations are mainly driven by the protrusive force generated by actin polymerization, which is localized to the leading edge of these protrusions. The adhesion is also essential for the formation of cohesive tissues, proliferation and also for cell motility. The formation of motile shapes is a very complex process that involves the reorganization and polarization of the cytoskeleton, the formation of focal adhesions, stress fibers etc. The actual shapes of the motile cells are, however, very diverse, ranging from half-moon like shapes of fish keratocytes to hand-like shapes of neuronal growth cones (Mogilner & Keren, 2009; Rafelski & Theriot, 2004).

In this review we present a simulation technique of Monte-Carlo simulations (MC) for predicting cell shapes due to isotropic inclusions and with combinations of active and adhesive forces. The review is structured as follows: We first discuss the theoretical basis for the numerical simulations and briefly describe the protocols that implement the theory on triangulated meshes. We go on to the simplest, so-called "passive" case, where there is no protrusive force and all morphologies stem from the thermodynamic mixing that minimizes the bending energy of the membrane and membrane inclusions. In this section, we identify regions of the phase space—defined by inclusion density and temperature—where shapes change from mixed to budded. The next section builds upon the model to include also protrusive forces at the sites of membrane inclusions. This leads to an interesting new class of pancake-like shapes that resemble lamellopodia with the majority of membrane inclusions found on the rim. The final section deals with the spreading of cells on extracellular substrates and leads to another new class of shapes called motile crescent shapes.

26.2 Simulation

The simulation consists of three parts: a numerical triangulation, which approximately describes the state of the physical system; an expression for the energy, derived from theoretical models that can be computed for any state of the data model; a time-evolution kernel that uses the energy to decide how to update the simulation from the current state to the next, in our case a Monte-Carlo method.

26.2.1 Model: triangulated surface

The lipid bilayer membrane is a thin sheet, so it can be approximated by a 2D surface, which is discretized by triangulation. Concretely, the membrane vesicle is represented by a set of N vertices that are linked by tethers of variable length l to form a closed, dynamically triangulated, self-avoiding two-dimensional network of approximately $2N$ triangles and with the topology of a sphere (Gompper & Kroll, 1996, 2004). The lengths of the tethers can vary between a minimal value $l_{\min}$ and a maximal value $l_{\max}$, which ensures the triangles do not become too needle-like: this is not too restrictive since the triangulation is dynamic: the fluid nature of the membrane requires dynamically modifying the triangulated mesh as part of the simulation. Thus, the data structure consists of two types of dynamical objects: The vertices, with their positions and the bonds, which can be destroyed and created.

To represent a 2D sheet, the network must not cross itself and must be self-avoidant: this is ensured by choosing the appropriate values for $l_{\max}$ and the maximal displacement of the vertex s in a single updating step and by rejecting any step where a vertex penetrates through the triangular network or that bond cuts through another. Proteins (and any other inclusion) are represented by a subset of N_c vertices with the rest representing the lipid membrane. The fraction of proteins to all vertices in the system is labeled as $\rho = N_c/N$.

26.2.2 Energy: Helfrich energy and protein interactions

The energy of lipid bilayer is typically described by the Helfrich expression (Helfrich, 1973, 1974):

$$W_b = \frac{\kappa}{2}\int_A (C_1 + C_2 - C_0)^2 dA. \tag{26.1}$$

At each point, the membrane has a spontaneous curvature C_0 and its shape is given by two principle curvatures C_1 and C_2. This energy penalizes local deviations from the optimal shape with a bending stiffness κ. For a membrane with the same composition of isotropic lipids on both sides, we expect $C_0 = 0$ (Kralj-Iglič et al., 2006), so at each point the membrane tends to minimize its curvature and remain flat, but global considerations, such as volume constraint and topology prevent the membrane from assuming its optimal shape at every point, leading to a variety of morphologies (Deuling & Helfrich, 1976). The complexity of the vesicle shape is driven by membrane inclusions, representing embedded proteins and external forces, representing the cytoskeleton and adhesive forces of the environment.

Following Gompper and Kroll (1996, 2004), the discrete version of Eq. (26.1) gives the bending energy:

$$W_b = \frac{\kappa}{2}\sum_{i\in\{N\}} \sigma_i (h_i - c_{0i})^2, \tag{26.2}$$

where σ_i is the area assigned to each vertex and h_i is the mean curvature. Vertices that represent curved membrane proteins (CMP) are given spontaneous curvature $C_0 = c_0$. Elsewhere we assume a symmetric membrane $C_0 = 0$.

Proteins tend to aggregate, which is modeled by nearest neighbor interaction: this gives the interaction energy:

$$W_{ij} = \begin{cases} -w & i,j \text{ are adjacent CMP} \\ 0 & \text{else} \end{cases} \tag{26.3}$$

Attractive interactions $w > 0$ induce phase separation of the lipid bilayer. In theoretical analysis, this corresponds to a ranged interaction (heaviside function) (Hägerstrand et al., 2006; Veksler & Gov, 2007).

Local protrusive forces from the cytoskeleton act on the CMP, producing work whenever they move:

$$W_F = -F \sum_i \hat{n}_i \cdot \delta\vec{r}_i, \tag{26.4}$$

where F is the size of the force, $\hat{n}_i$ is the outwards normal to the membrane at the location of the protein i and $\delta\vec{r}_i$ is a displacement of the CMP vertex i. The sum runs over all proteins. This normal force term in the energy has the form of a fictitious external potential pulling on each protein in the direction of the instantaneous outwards normal.

26.2.3 Method: the Monte-Carlo algorithm

One Monte-Carlo sweep (MCs) consists of individual attempts to displace each of the N vertices by a random increment in the sphere with radius s, centered at the vertex, followed by $R_B N$ attempts to flip a randomly chosen bond. We denote R_B as the bond-flip ratio, which defines how many attempts to flip a bond are made per one attempt to move a vertex in one MCs. Note that the bond-flip ratio is connected to the lateral diffusion coefficient within the membrane, i.e. to the membrane viscosity (Bivas et al., 1987). In our works we have chosen $R_B = 3$, $s/l_{\min} = 0.15$ and $l_{\max}/l_{\min} = 1.7$. It is this bond-flip mechanism that gives the dynamically triangulated network its lateral fluidity. A single bond-flip involves the four vertices of two neighboring triangles. The tether connecting the two vertices in diagonal direction is cut and reestablished between the other two, previously unconnected, vertices. In Fig. 26.1A, the triangulation method is shown for a smooth

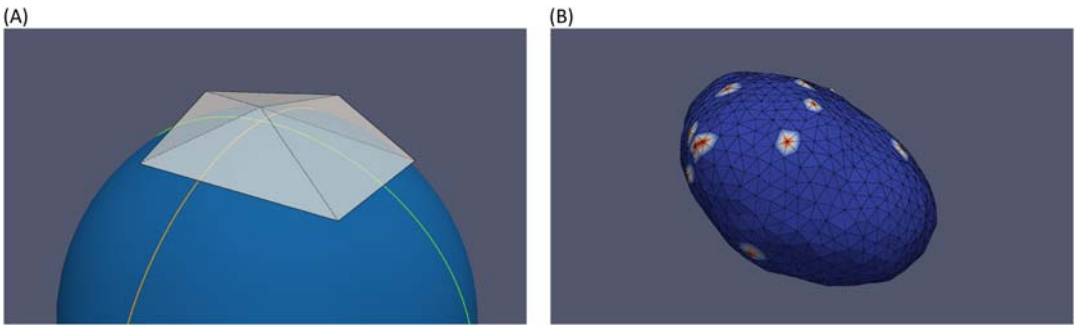

FIGURE 26.1 (A) Curvatures at a vertex are determined by fitting a spherical surface: $C_1 = \frac{1}{R_1}$ and $C_2 = \frac{1}{R_2}$. The spontaneous curvature has a tendency to assume a dome-like shape with radius $R = \frac{1}{C_0}$. (B) A snap-shot of a typical simulation result with the membrane represented in blue and CMP with red.

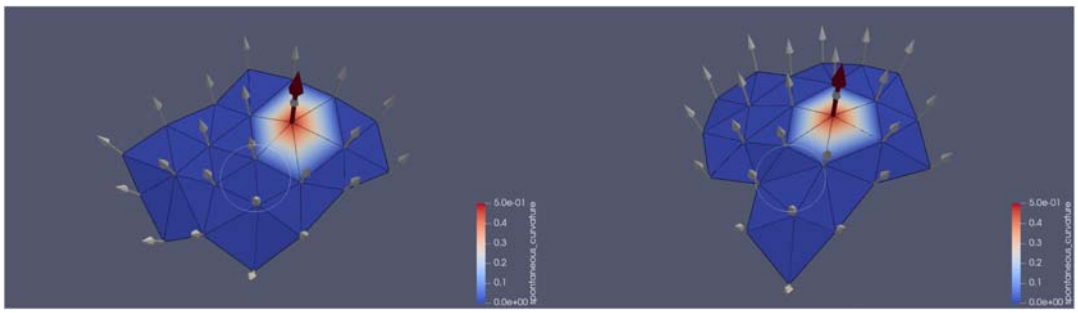

FIGURE 26.2 Small patch of the vesicle at two instances, separated by a hundred MC steps: white arrows are the normals of the vertices and red arrow is the force on the CMP vertex which is in the normal direction. Highlighted in white circle is a bond-flip that occurred between the steps. The color legend denotes the spontaneous curvature.

spherical surface, while a typical snap-shot of a simulated vesicle is shown in Fig. 26.1B. In the active case, the normal forces at the sites of CMP are shown in Fig. 26.2.

26.3 Results and discussion

26.3.1 Membranes shaped by passive curved membrane proteins

Fig. 26.3A and B show a phase diagram with snap-shots of typical shapes of vesicles that contain passive CMP in the absence of active protrusive forces. The system is in thermal equilibrium at different temperatures and densities (area coverage fraction $\rho = N_c/N$) of CMP with the spontaneous curvature of membrane inclusions $c_0 = 0.5/l_{\min}$. An increase in temperature leads to a fluid membrane with larger shape fluctuations and fast rate of protein-protein unbinding, promoting protein mixing and a homogeneous protein distribution (the top left corner of Fig. 26.3A and B shows approximately spherical morphologies). Conversely, a decrease in temperature increases the tendency of proteins to cluster together, forming buds and lobes whose effective radii are similar to the spontaneous curvature c_0.

For a qualitative measure of the protein cluster size we measure the average number of proteins included in clusters by the equation (Fošnarič et al., 2019):

$$\langle \overline{N}_{\mathrm{vc}} \rangle = \left\langle \frac{\sum_i N_{\mathrm{vc}}^{(i)} N_{\mathrm{cl}}^{(i)}}{\sum_i N_{\mathrm{cl}}^{(i)}} \right\rangle. \tag{26.5}$$

Here, the angle brackets denote the canonical ensemble average. At any given time during the simulation, $\overline{N}_{\mathrm{vc}}$ is the mean cluster size and the sums run over all clusters of vertices representing proteins. In the sums, $N_{\mathrm{vc}}^{(i)}$ is the number of vertices in cluster i and $N_{\mathrm{cl}}^{(i)}$ is the number of clusters of size $N_{\mathrm{vc}}^{(i)}$. The cluster increase in size with increasing density of CMP (Fig. 26.3C).

We compare the simulation results with the prediction of linear stability analysis (Fošnarič et al., 2019; Gladnikoff et al., 2009). Linear stability analysis predicts a critical

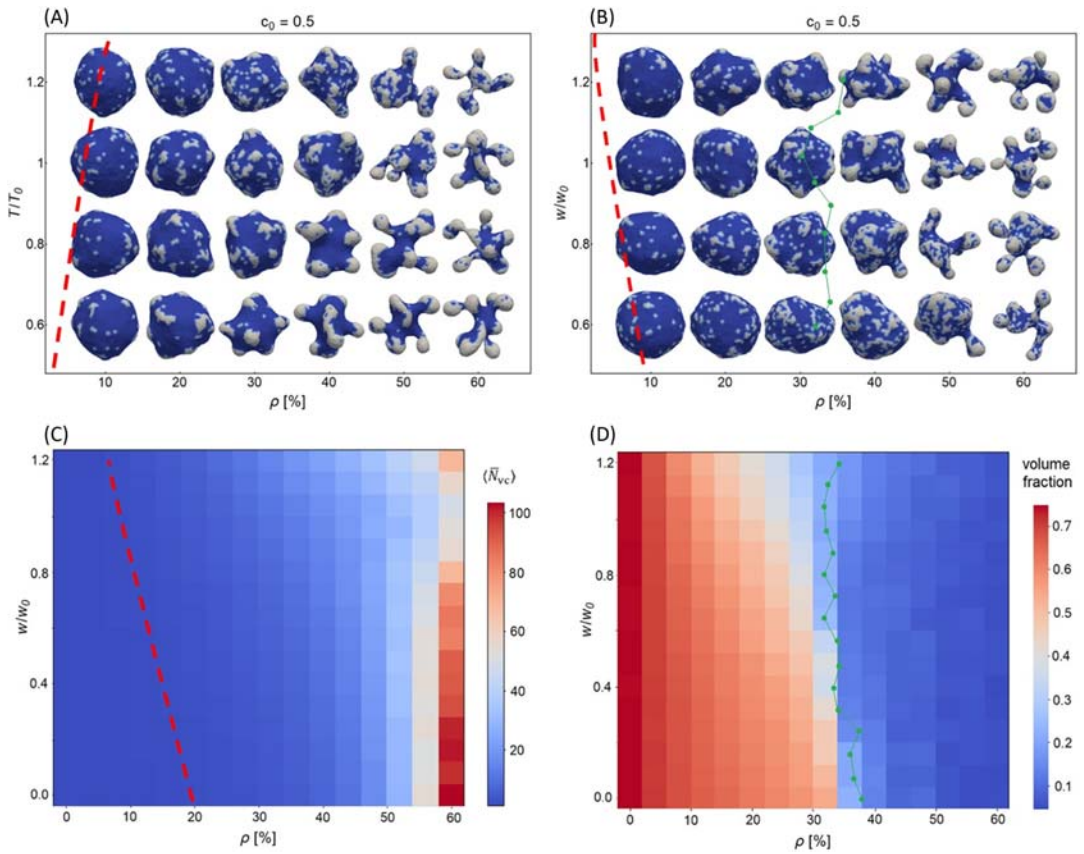

FIGURE 26.3 A phase diagram of microstates of vesicles with spontaneous curvature $c_0 = 0.5/l\text{min}$ and no protrusive force in the T (ρ) plane (A) and the $w(\rho)$ plane (B). The patches of flat membrane with no spontaneous curvature are shown in dark blue, while the gray areas correspond to positive spontaneous curvature c_0. Increasing the temperature at constant protein density promotes mixing and ensures a homogeneous distribution of proteins. At high protein densities, proteins aggregate into necklace-like protrusions, resembling a budding membrane. (C) The average number of proteins in the clusters (Eq. 26.5) given for the phase diagram in the $w(\rho)$ plane. (D) The volume fraction of a vesicle in relation to the bounding sphere. At low CMP denisities, the morphologies tend to be quasispherical. The red dashed line in all three panels corresponds to the critical temperature $T^{(c)}$ (Eq. 26.6) where $\langle \overline{N}_{\text{vc}} \rangle = 2$. The green line in panels (B) and (D) gives an approximate value where the volume fraction is 20%.

thermal energy, $k_B T^{(c)}$, below which the instability occurs and buds start to form. In thermal equilibrium and in the absence of protrusive forces, the critical temperature $T^{(c)}$ is (Fošnarič et al., 2019):

$$T^{(c)} = \frac{12w}{k_B}(1-\rho)\rho. \tag{26.6}$$

The critical temperature is plotted in Fig. 26.3 and corresponds to the line where $\langle \overline{N}_{\text{vc}} \rangle = 2$ (Fig. 26.3C).

As the vesicles grow more buds and deviate from quasispherical, their volume decreases. Comparing a vesicle's volume to a volume of a bounding sphere with a radius that corresponds to the maximum distance of a vertex from the center of the vesicle gives a volume fraction that can be plotted as a heat map in the $w(\rho)$ plane (Fig. 26.3D). The region of highly budded morphologies is found across the line where the volume fraction decreases below a certain threshold value, for example 20% (green line in Fig. 26.3B and D).

At low average protein densities the equilibrium vesicle shapes remain quasispherical, with clusters that increase in size with decreasing temperature. At higher average protein densities cluster sizes increase and curved protein buds appear on the membrane, splitting the phase diagram into mixed and budded morphologies. These budded, necklace-like structures form because curved proteins cannot form flat aggregates due to their spontaneous curvature (see right column of Fig. 26.3B). Necklace-like membrane protrusions have been observed in cellular membranes (Heinrich et al., 2014) and in many in vitro experiments (Bhatia et al., 2020; Drab et al., 2021; Tsafrir et al., 2001; Yu & Granick, 2009).

26.3.2 Membranes shaped by curved membrane protein that recruit protrusive forces

With the addition of active protrusive forces at the sites of CMP the system is not in thermodynamic equilibrium any more, and the steady-state shapes do not arise from a simple minimization of bending and protein-protein binding energies.

The addition of active forces promotes demixing and shifts the transition from mixed to budded morphologies to higher temperatures and lower protein densities (Fig. 26.4A). A more dramatic consequence of protrusive forces is seen at low temperatures and protein concentrations – there is a transition into a new class of pancake-like shapes that were not observed in the equilibrium morphologies without active forces (see Fig. 26.4A).

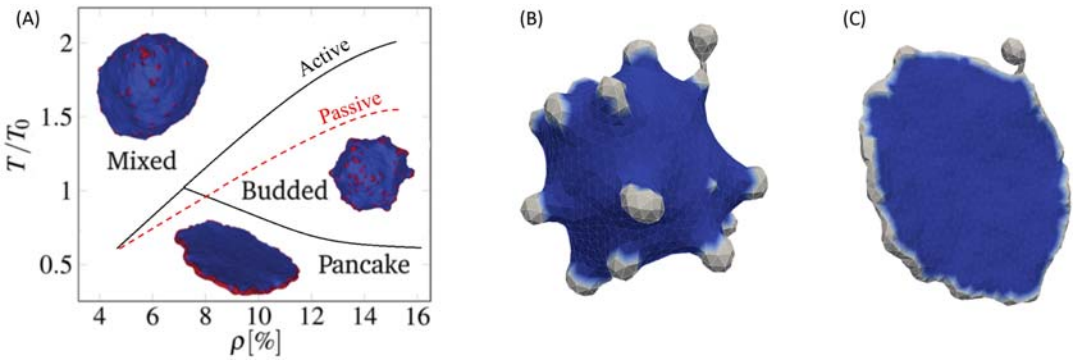

FIGURE 26.4 (A) Approximate temperatures below which a transition into budded and pancake shapes in the simulations for both active (black) and passive (red) cases. (B) An example of a small pearling protrusion in the passive case for the parameters $c_0 = 0.5/l\text{min}$, $w/w_0 = 2$ and $\rho = 0.2$. (C) A small pearling protrusion found on the rim as a direct consequence of CMP crowding in the pancake phase ($c_0 = 1/l\text{min}$, $w/w_0 = 3$, $\rho = 0.19$ and $F = 1\ k_BT_0/l\text{min}$). Source: *Adapted from Fošnarič M., Penič S., Iglič A., Kralj-Iglič V., Drab M., Gov N.S., (2019). Theoretical study of vesicle shapes driven by coupling curved proteins and active cytoskeletal forces*, Soft Matter, 15*(26), 5319–5330.*

The transition from deformed-spherical to pancake-like shapes is seen in Fig. 26.4A as the split in the transition line in the T (ρ) diagram. The CMP cluster forming a closed ring along the rim of the pancake shape is highly stable and effective in stretching out the flat membrane parts. The stretching of the membrane in these regions also acts to suppress aggregation of the CMP there. The flat sides of the pancake-shaped vesicles are devoid of proteins since these regions are energetically unfavorable for the curved proteins.

At low protein densities there are not enough CMP to form a closed ring-like cluster around the rim of the flattened vesicle and the system changes into a new class of two-arc shapes (Fig. 26.5). The curved proteins form arc-like clusters that line the flattened ends of an elongated vesicle. At large protein densities the excess proteins crowd the rim and cause it to undergo buckling and curling. At the highest densities, these excess proteins extend from the closed ring cluster in the form of spherical and necklace-like clusters, as also seen in the passive case (Fig. 26.4B and C). An interesting class of morphologies is found in the case of flat CMP with $c_0 = 0$ and protrusive forces. These highly elongated protrusions are driven by the protrusive force provided by a cluster of proteins at the protrusion's tip and can be understood by force balance between the protrusive force provided by the protein cluster at the tip and the elastic restoring force due to membrane bending (for a detailed analysis, see Fošnarič et al. (2019)). In this phase the shapes are highly unstable and dynamic, with protrusions merging and growing.

Note that our current model does not allow vesicle fission, and the topology of the vesicle remains fixed. The formation of buds in real cells (Fig. 26.4B–C) leads to the accumulation of topological defects around the neck that have high energy cost (Penič, Mesarec, et al., 2020). These defects, when accumulated is a very small area weakened the neck, resulting in neck rupture and the fission of cells into small parts (Gongadze et al., 2021) (Fig. 26.6).

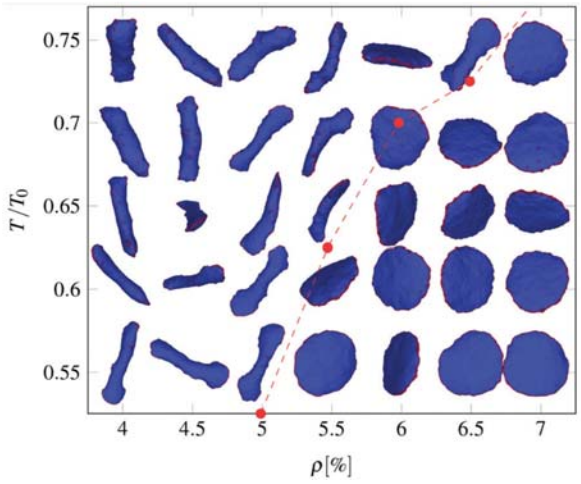

FIGURE 26.5 Final microstates of vesicles with protrusive force in the case of low protein densities reveal the transition from pancake-like to arc-like shapes. The transition is approximately given by the red line. Source: *Adapted part (A) from Fošnarič M., Penič S., Iglič A., Kralj-Iglič V., Drab M., Gov N.S., (2019). Theoretical study of vesicle shapes driven by coupling curved proteins and active cytoskeletal forces,* Soft Matter, 15*(26), 5319–5330.*

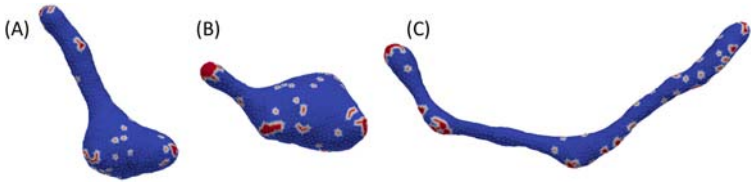

FIGURE 26.6 Final microstates of vesicles with protrusive force in the case of flat CMP ($c_0 = 0$) at different CMP densities: (A) $\rho = 0.07$, (B) $\rho = 0.1$ and (C) $\rho = 0.14$. For all cases, $w/w_0 = 1$ and $F = 4\ k_B T_0/l$min.

26.3.3 Cell spreading and motility

Cells adhere to extracellular matrices during the normal development of the organism or during cell motility. The present model could easily be extended to study the spreading and motility on an extracellular substrate (Sadhu et al., 2021). We consider a flat surface over which we place the vesicle with which it has an attractive interaction. The extra attractive interaction adds one more term to the total energy (Eqs. 26.1, 26.3 and 26.4), i.e., the adhesion energy, which in its simplest form is given by:

$$W_A = -\sum_{i'} E_{ad}, \tag{26.7}$$

where E_{ad} is the adhesion strength, defined as the adhesion energy per adhered vertex and the sum runs over all the vertices that are adhered on the extracellular substrate. A membrane vertex is adhered if it is found within a short distance (ε) from the adhesive substrate.

For a vesicle with passive proteins, the adhered area increases with protein density (Fig. 26.7A). The proteins aggregate around the highly curved rim and reduce the bending energy. This reduction in bending energy allows the vesicle to adhered more and thereby increases the adhered area (Sadhu et al., 2021). For a vesicle with active proteins, an increase in the active protrusive force F increases the adhered area (Fig. 26.7B). For large F, if the protein density is sufficient to form a closed ring-like aggregate around the vesicle rim, the vesicle shape becomes pancake-like (Sadhu et al., 2021). These pancake shapes correspond to those cells that efficiently spread on surfaces using lamellipodia. The presence of curved proteins and active forces allows them to spread on surfaces with low adhesion strength (low E_{ad}), so that they can easily deadhere if needed (such as during cell division, for example). Similar pancake-like shape is also observed without adhesion, but the transition to this shape is observed at higher protein density (Fošnarič et al., 2019).

For small protein density, where there are not enough proteins to form a closed ring-like aggregate around the cell rim (pancake shape), we mainly obtain two types of shapes, (1) two-arc shapes that are nonmotile (Fig. 26.7C-i) and (2) crescent-like shapes that are motile (Fig. 26.7C-ii). By "motile," we mean that the active CMP form a single large aggregate on one side of the vesicle that results in an unbalanced force that pushes the vesicle along the adhesive substrate. The motile shapes in our model are obtained by spontaneous symmetry breaking that is driven by self-organization of the active CMP and the membrane shape. We obtain this phenotype with only a minimal set of ingredients: adhesion of sufficient strength and the CMP coupled with the protrusive forces. These motile shapes are very similar to the shapes of different motile cells observed in experiments (Mogilner & Keren, 2009;

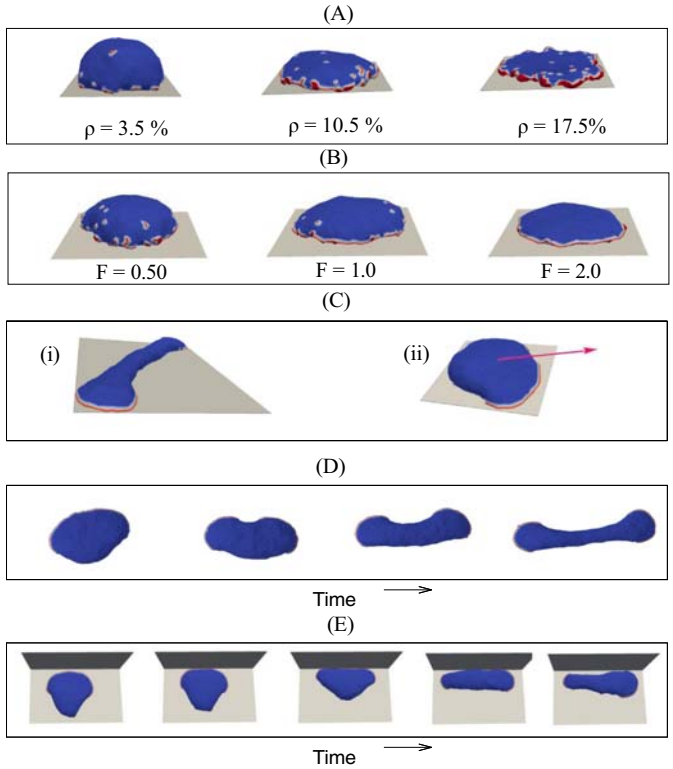

FIGURE 26.7 Different shapes of vesicles spreading over flat adhesive substrates. (A) Spreading of a vesicle with passive proteins. The adhered area increases as we increase the protein density (ρ). Here we use $E_{ad} = 0.75\ k_BT$. (B) Spreading of a vesicle with active proteins. The adhered area increases with F, and becomes pancake-like for large F. Other parameters are $E_{ad} = 0.50\ k_BT$ and $\rho = 0.07$ (C-i) In the small density regime, when the density of proteins are not enough to form a closed circular rim, nonmotile two-arc shapes are formed. (C-ii) In the small density regime, another shape is possible, where all the proteins aggregate into one single cluster, that gives rise to a crescent-shaped motile vesicle. Here we use $E_{ad} = 2.0$, $\rho = 0.035$ and $F = 4.0\ k_BT/l_{min}$. (D) A crescent-shaped vesicle can spontaneously break into a two-arc shape in the long time limit. (E) Similar breaking of the crescent shape into a two-arc is also possible, when the crescent vesicle is perturbed externally, such as, hitting a barrier placed vertically in front of it. For all the results, the total number of vertices are $N = 1447$ and $c_0 = 1\ l^{-1}_{min.}$

Rafelski & Theriot, 2004). Real cell motility is, however, a more complex process which is modulated by a range of biochemical and biophysical signals, both extracellular and intracellular.

The obtained motile shapes are fragile and the single protein aggregate may sometime break into two parts, forming an elongated two-arc shape (Fig. 26.7D). This spontaneous conversion from a single leading-edge to the two-arc shape is reminiscent of very similar dynamics observed in motile cells (Neilson et al., 2011). The motile vesicle can also break when exposed to external perturbations, such as hitting a barrier (Fig. 26.7E). After breaking into two-arc shapes, the vesicle could not regain its motile property back and remained in the two-arc shape. In real cells, however, there are mechanisms which enable it to

regain its motility by repolarizing. Specifically, as cells in the two-arc shape elongate beyond a critical length, they are likely to polarize, with one of the leading-edges (CMP arcs) inhibiting the other (Ron et al., 2020).

It is clear from these results that the two-arc and a crescent shapes can coexist with each other in the same parameter regime. To quantify this we show a phase diagram in the adhesion-strength vs protrusive force (E_{ad} - F) plane in Fig. 26.8, indicating all the steady-state shapes. The color shading is showing the probability to obtain a motile crescent shape. The black regions represent zero probability to obtain a crescent shape while a yellow color indicates a region with only crescent shapes. For small E_{ad} and F, the proteins do not form large clusters. In this regime, the proteins form disordered small clusters, and the vesicle remains approximately hemispherical. For very large force we have mostly two-arc shapes, as the active energy dominates over the adhesion energy and stretches the vesicle into an elongated two-arc shape and gains maximum active work. In the large E_{ad} and small F region, we mostly have crescent shapes, where adhesion energy is mainly driving the aggregation of proteins into a single cluster, which efficiently spreads the vesicle and increases its adhered surface. However, there is a large regime, where the crescent and two-arc shapes coexists with each other.

We separate different regimes by simulation points and by lines from analytical predictions (Sadhu et al., 2021). The yellow points and line separate the two regimes above which we have no probability to obtain a crescent shape and below which we have a finite probability to obtain a crescent shape. The green points and line separates the regime below which we only obtain quasispherical shapes and above which we have either a crescent or a two-arc shape.

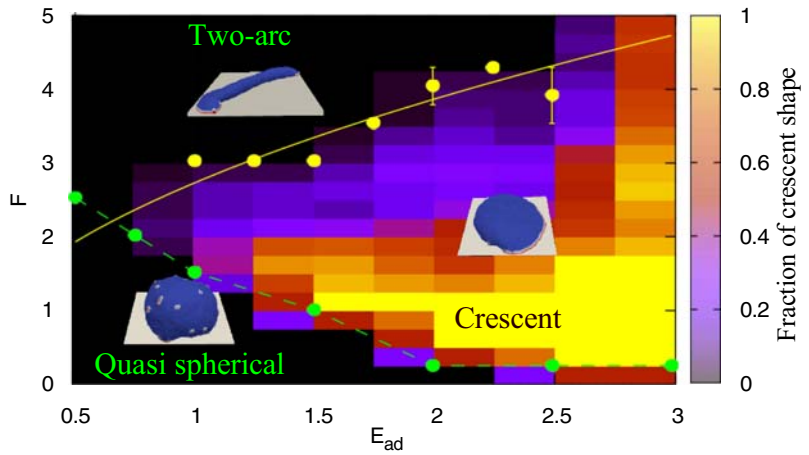

FIGURE 26.8 Phase diagram of all possible shapes in the small protein density limit. The background color is showing the probability of having a crescent-shape. In the small E_{ad} region, we mainly have quasispherical shapes. In the large force regime, two-arc shapes are most likely. In the large E_{ad} regime, there is a large region, where crescent shapes are obtained. The probability of having a crescent is close to unity for large E_{ad} and small F. The yellow line and point separates the region, above which we only have the possibility to obtain a two-arc shape. The green line and points separates the region below which we have quasispherical shapes and above which we have either a crescent shape or a two-arc shape.

We can now utilize these theoretical predictions to explain some experimental observations. Our prediction for the transition line from two-arc to crescent shape (yellow point and line) may explain the observation made in (Spence et al., 2012), where knocking-down one of the actin nucleators, which may be considered as reducing the overall protrusive force F, had a similar effect on the shape and motility of cells, i.e., the knocking-down cells were more motile compared to that without knocking-down cells. A similar observation was made in (Pankov et al., 2005), where decreasing the amount of Rac-GTPase, which activates downstream actin nucleators (Sit & Manser, 2011), stabilizes a single leading edge and converts the cells to have more persistent motility. The lower transition line (green points and line) can be compared to the experimentally observed loss of motility below a critical surface coverage of adhesive substrate (Maheshwari et al., 2000).

26.4 Conclusions

In this review we have presented Monte-Carlo simulations of vesicle shapes and their coupling of convex curved membrane proteins that also have the ability to recruit the protrusive forces of the cytoskeleton. In living organisms, these forces are most commonly provided by the cytoskeleton due to actin polymerization, which is directed to the cell membrane by a variety of protein complexes. We have identified the main classes of shapes in the phase diagram for the passive case, where CMP clusters leading to membrane budding was observed. In the case of active protrusive forces, we have identified another class of pancake-like shapes and elongated two-arc like shapes at low protein densities.

Furthermore, we have shown that interacting CMP, passive and active, affect the process of vesicle spreading and adhesion. Large density of passive curved proteins can greatly enhance the adhesion of vesicles on low adhesion substrates. Coupling the curved proteins with active protrusive forces extends this enhancement to lower densities of curved proteins. By spontaneously self-organizing curved proteins at the cell−substrate contact line, the active forces drive a shape transition into a flat geometry with high adhered area and robust spreading. At very low densities of curved proteins, the protrusive activity can stabilize either spindle-like elongated cells, or motile crescent shapes.

The aggregation and budding due to the recruited active forces of the cytoskeleton have important consequences for a variety of biological processes, such as budding of viruses and initiation of cellular protrusions (such as lamellipodia and filopodia) during development and cell motility. This review highlights the rich variety of membrane shapes that are induced by CMP that recruit the active forces of the cytoskeleton, which are indeed utilized by living cells during different biological processes. Although the cell is far more complex than is represented by this model, the model describes a large spectrum of observed cellular shapes that allow us to gain deep understanding of the relationship between the cell shape and the underlying forces that shape it.

References

Alimohamadi, H., Smith, A. S., Nowak, R. B., Fowler, V. M., & Rangamani, P. (2020). Non-uniform distribution of myosin-mediated forces governs red blood cell membrane curvature through tension modulation. *PLoS Computational Biology*, *16*(5), e1007890.

Baumgart, T., Capraro, B. R., Zhu, C., & Das, S. L. (2011). Thermodynamics and mechanics of membrane curvature generation and sensing by proteins and lipids. *Annual Review of Physical Chemistry*, *62*, 483–506.
Bhatia, T., Christ, S., Steinkühler, J., Dimova, R., & Lipowsky, R. (2020). Simple sugars shape giant vesicles into multispheres with many membrane necks. *Soft Matter*, *16*(5), 1246–1258.
Bivas, I., Hanusse, P., Bothorel, P., Lalanne, J., & Aguerre-Chariol, O. (1987). An application of the optical microscopy to the determination of the curvature elastic modulus of biological and model membranes. *Journal de Physique*, *48*(5), 855–867.
Boulbitch, A. (1998). Deflection of a cell membrane under application of a local force. *Physical Review E*, *57*(2), 2123.
Božič, B., Kralj-Iglič, V., & Svetina, S. (2006). Coupling between vesicle shape and lateral distribution of mobile membrane inclusions. *Physical Review E*, *73*(4), 041915.
Cavalcanti-Adam, E. A., Volberg, T., Micoulet, A., Kessler, H., Geiger, B., & Spatz, J. P. (2007). Cell spreading and focal adhesion dynamics are regulated by spacing of integrin ligands. *Biophysical Journal*, *92*(8), 2964–2974.
Cevc, G., & Marsh, D. (1987). *Phospholipid bilayers: Physical principles and models*. Wiley.
Cuvelier, D., Théry, M., Chu, Y.-S., Dufour, S., Thiéry, J.-P., Bornens, M., Nassoy, P., & Mahadevan, L. (2007). The universal dynamics of cell spreading. *Current Biology*, *17*(8), 694–699.
Deuling, H., & Helfrich, W. (1976). The curvature elasticity of fluid membranes: A catalogue of vesicle shapes. *Journal de Physique*, *37*(11), 1335–1345.
Discher, D. E. (2018). *Biomembrane mechanical properties direct diverse cell functions. Physics of biological membranes* (pp. 263–285). Springer.
Döbereiner, H.-G., Dubin-Thaler, B., Giannone, G., Xenias, H. S., & Sheetz, M. P. (2004). Dynamic phase transitions in cell spreading. *Physical Review Letters*, *93*, 108105.
Drab, M., Pandur, Ž., Penič, S., Iglič, A., Kralj-Iglič, V., & Stopar, D. (2021). A Monte-Carlo study of giant vesicle morphologies in nonequilibrium environments. *Biophysical Journal*, *120*, 4418–4428.
Drab, M., Stopar, D., Kralj-Iglič, V., & Iglič, A. (2019). Inception mechanisms of tunneling nanotubes. *Cells*, *8*(6), 626.
Evans, E., & Skalak, R. (1980). *Mechanics and thermodynamics of biomembranes. 1980*. Boca Raton, FL: CRC.
Fošnarič, M., Iglič, A., & May, S. (2006). Influence of rigid inclusions on the bending elasticity of a lipid membrane. *Physical Review E*, *74*(5), 051503.
Fošnarič, M., Penič, S., Iglič, A., Kralj-Iglič, V., Drab, M., & Gov, N. S. (2019). Theoretical study of vesicle shapes driven by coupling curved proteins and active cytoskeletal forces. *Soft Matter*, *15*(26), 5319–5330.
Gauthier, N. C., Fardin, M. A., Roca-Cusachs, P., & Sheetz, M. P. (2011). Temporary increase in plasma membrane tension coordinates the activation of exocytosis and contraction during cell spreading. *Proceedings of the National Academy of Sciences*, *108*(35), 14467–14472.
Gladnikoff, M., Shimoni, E., Gov, N. S., & Rousso, I. (2009). Retroviral assembly and budding occur through an actin-driven mechanism. *Biophysical Journal*, *97*(9), 2419–2428.
Gompper, G., & Kroll, D. (1996). Random surface discretizations and the renormalization of the bending rigidity. *Journal de Physique I*, *6*(10), 1305–1320.
Gompper, G., & Kroll, D. (2004). *Triangulated-surface models of fluctuating membranes. Statistical Mechanics of Membranes and Surfaces* (pp. 359–426). World Scientific.
Gongadze, E., Mesarec, L., Kralj, S., Kralj-Iglič, V., & Iglič, A. (2021). On the role of electrostatic repulsion in topological defect-driven membrane fission. *Membranes*, *11*(11), 812.
Gov, N. (2018). Guided by curvature: Shaping cells by coupling curved membrane proteins and cytoskeletal forces. *Philosophical Transactions of the Royal Society B: Biological Sciences*, *373*(1747), 20170115.
Graziano, B. R., Town, J. P., Sitarska, E., Nagy, T. L., Fošnarič, M., Penič, S., Iglič, A., Kralj-Iglič, V., Gov, N. S., Diz-Muñoz, A., & Weiner, O. D. (2019). Cell confinement reveals a branched-actin independent circuit for neutrophil polarity. *PLoS Biology*, *17*(10), e3000457.
Hägerstrand, H., Mrowczynska, L., Salzer, U., Prohaska, R., Michelsen, K. A., Kralj-Iglič, V., & Iglič, A. (2006). Curvature-dependent lateral distribution of raft markers in the human erythrocyte membrane. *Molecular Membrane Biology*, *23*(3), 277–288.
Heinrich, D., Ecke, M., Jasnin, M., Engel, U., & Gerisch, G. (2014). Reversible membrane pearling in live cells upon destruction of the actin cortex. *Biophysical Journal*, *106*(5), 1079–1091.
Helfrich, W. (1973). Elastic properties of lipid bilayers: Theory and possible experiments. *Zeitschrift für Naturforschung C*, *28*(11–12), 693–703.
Helfrich, W. (1974). Blocked lipid exchange in bilayers and its possible influence on the shape of vesicles. *Zeitschrift für Natur - Forschung C*, *29*(9–10), 510–515.

Iglič, A. (1997). A possible mechanism determining the stability of spiculated red blood cells. *Journal of Biomechanics*, *30*(1), 35–40.
Iglič, A., Babnik, B., Bohinc, K., Fošnarič, M., Hägerstrand, H., & Kralj-Iglič, V. (2007). On the role of anisotropy of membrane constituents in formation of a membrane neck during budding of a multicomponent membrane. *Journal of Biomechanics*, *40*(3), 579–585.
Iglič, A., Kralj-Iglič, V., & Hagerstrand, H. (1998). Amphiphile induced echinocyte-spheroechinocyte transformation of red blood cell shape. *European Biophysics Journal*, *27*(4), 335–339.
Iglič, A., Lokar, M., Babnik, B., Slivnik, T., Veranič, P., Hägerstrand, H., & Kralj-Iglič, V. (2007). Possible role of flexible red blood cell membrane nanodomains in the growth and stability of membrane nanotubes. *Blood Cells, Molecules, and Diseases*, *39*(1), 14–23.
Israelachvili, J. N. (2011). *Intermolecular and surface forces* (3rd Edition). Academic press.
Kozlov, M. M., Campelo, F., Liska, N., Chernomordik, L. V., Marrink, S. J., & McMahon, H. T. (2014). Mechanisms shaping cell membranes. *Current Opinion in Cell Biology*, *29*, 53–60.
Kralj-Iglič, V., Babnik, B., Gauger, D. R., May, S., & Iglič, A. (2006). Quadrupolar ordering of phospholipid molecules in narrow necks of phospholipid vesicles. *Journal of Statistical Physics*, *125*(3), 727–752.
Kralj-Iglič, V., Heinrich, V., Svetina, S., & Žekš, B. (1999). Free energy of closed membrane with anisotropic inclusions. *The European Physical Journal B-Condensed Matter and Complex Systems*, *10*(1), 5–8.
Leibler, S. (1986). Curvature instability in membranes. *Journal de Physique*, *47*(3), 507–516.
Lim H.W., G., Wortis, M., & Mukhopadhyay, R. (2002). Stomatocyte-discocyte-echinocyte sequence of the human red blood cell: Evidence for the bilayer-couple hypothesis from membrane mechanics. *Proceedings of the National Academy of Sciences*, *99*(26), 16766–16769.
Maheshwari, G., Brown, G., Lauffenburger, D. A., Wells, A., & Griffith, L. G. (2000). Cell adhesion and motility depend on nanoscale rgd clustering. *Journal of Cell Science*, *113*(10), 1677–1686.
Markin, V. (1981). Lateral organization of membranes and cell shapes. *Biophysical Journal*, *36*(1), 1–19.
Mogilner, A., & Keren, K. (2009). The shape of motile cells. *Current Biology*, *19*(17), R762–R771.
Mohandas, N., & Evans, E. (1994). Mechanical properties of the red cell membrane in relation to molecular structure and genetic defects. *Annual Review of Biophysics and Biomolecular Structure*, *23*(1), 787–818.
Neilson, M. P., Veltman, D. M., van Haastert, P. J. M., Webb, S. D., Mackenzie, J. A., & Insall, R. H. (2011). Chemotaxis: A feedback- based computational model robustly predicts multiple aspects of real cell behaviour. *PLoS Biology*, *9*(5), 1–11.
Pankov, R., Endo, Y., Even-Ram, S., Araki, M., Clark, K., Cukierman, E., Matsumoto, K., & Yamada, K. M. (2005). A rac switch regulates random vs directionally persistent cell migration. *The Journal of Cell Biology*, *170*(5), 793–802.
Penič, S., Fošnarič, M., Mesarec, L., Iglič, A., & Kralj-Iglič, V. (2020). Active forces of myosin motors may control endovesiculation of red blood cells. *Acta Chimica Slovenica*, *67*(2), 674–681.
Penič, S., Mesarec, L., Fošnarič, M., Mrówczyńska, L., Hägerstrand, H., Kralj-Iglič, V., & Iglič, A. (2020). Budding and fission of membrane vesicles: A mini review. *Frontiers in Physics*, *8*, 342.
Rafelski, S. M., & Theriot, J. A. (2004). Crawling toward a unified model of cell motility: Spatial and temporal regulation of actin dynamics. *Annual Review of Biochemistry*, *73*(1), 209–239.
Rodríguez-García, R., López-Montero, I., Mell, M., Egea, G., Gov, N. S., & Monroy, F. (2015). Direct cytoskeleton forces cause membrane softening in red blood cells. *Biophysical Journal*, *108*(12), 2794–2806.
Ron, J. E., Monzo, P., Gauthier, N. C., Voituriez, R., & Gov, N. S. (2020). One-dimensional cell motility patterns. *Physical Review Research*, *2*, 033237.
Sackmann, E. (1990). Molecular and global structure and dynamics of membranes and lipid bilayers. *Canadian Journal of Physics*, *68*(9), 999–1012.
Sadhu, R. K., Penič, S., Iglič, A., & Gov, N. S. (2021). Modeling cellular spreading and emergence of motility in the presence of curved membrane proteins and active cytoskeleton forces. *The European Physical Journal Plus*, *136*(5), 1–37.
Sit, S.-T., & Manser, E. (2011). Rho GTPases and their role in organizing the actin cytoskeleton. *Journal of Cell Science*, *124*(5), 679–683.
Smith, A. S., Nowak, R. B., Zhou, S., Giannetto, M., Gokhin, D. S., Papoin, J., Ghiran, I. C., Blanc, L., Wan, J., & Fowler, V. M. (2018). Myosin iia interacts with the spectrin-actin membrane skeleton to control red blood cell membrane curvature and deformability. *Proceedings of the National Academy of Sciences*, *115*(19), E4377–E4385.

Spence, H. J., Timpson, P., Tang, H. R., Insall, R. H., & Machesky, L. M. (2012). Scar/wave3 contributes to motility and plasticity of lamellipodial dynamics but not invasion in three dimensions. *The Biochemical Journal*, *448*(1), 35–42.

Tsafrir, I., Sagi, D., Arzi, T., Guedeau-Boudeville, M.-A., Frette, V., Kandel, D., & Stavans, J. (2001). Pearling instabilities of membrane tubes with anchored polymers. *Physical Review Letters*, *86*(6), 1138.

Veksler, A., & Gov, N. S. (2007). Phase transitions of the coupled membrane-cytoskeleton modify cellular shape. *Biophysical Journal*, *93*(11), 3798–3810.

Yu, Y., & Granick, S. (2009). Pearling of lipid vesicles induced by nanoparticles. *Journal of the American Chemical Society*, *131*(40), 14158–14159.